Article

Initial Drift Correction and Spectral Calibration of MarSCoDe Laser-Induced Breakdown Spectroscopy on the Zhurong Rover

Liangchen Jia [1], Xiangfeng Liu [2,*], Weiming Xu [1,2], Xuesen Xu [1], Luning Li [2], Zhicheng Cui [1], Ziyi Liu [1] and Rong Shu [1,2]

1 School of Physics and Optoelectronic Engineering, Hangzhou Institute for Advanced Study, University of Chinese Academy of Sciences, Hangzhou 310024, China
2 Key Laboratory of Space Active Opto-Electronics Technology, Shanghai Institute of Technical Physics, Chinese Academy of Sciences, Shanghai 200083, China
* Correspondence: liuxiangfeng@mail.sitp.ac.cn

Abstract: The Mars Surface Composition Detector (MarSCoDe) carried by the Zhurong rover of China's Tianwen-1 mission uses Laser-Induced Breakdown Spectroscopy (LIBS) to detect and analyze the material composition on Martian surfaces. As one extraterrestrial remote LIBS system, it is necessary to adopt effective and reliable preprocessing methods to correct the spectral drift caused by the changes in environmental conditions, to ensure the analysis accuracy of LIBS scientific data. This paper focuses on the initial spectral drift correction and estimates the accuracy of on-board wavelength calibration on the LIBS calibration target measured by the MarSCoDe LIBS. There may be two cases during the instrument launch and landing, as well as the long-term operation: (a) the initial wavelength calibration relationship can still apply to the on-board LIBS measurement; and (b) the initial wavelength calibration relationship has been changed, and a new on-board calibration is needed to establish the current relationship. An approach of matching based on global iterative registration (MGR) is presented in respect to case (a). It is also compared with the approach of particle swarm optimization (PSO) for case (b). Furthermore, their accuracy is estimated with the comparison to the National Institute of Standards and Technology (NIST) database. The experimental results show that the proposed approach can effectively correct the drift of the on-board LIBS spectrum. The the root-mean-square error (RMSE) of the internal accord accuracy for three channels is 0.292, 0.223 and 0.247 pixels, respectively, compared with the corrected Ti-alloy spectrum and the NIST database, and the RMSE of the external accord accuracy is 0.232, 0.316 and 0.229 pixels, respectively, for other samples. The overall correction accuracy of the three channels is better than one-third of the sampling interval.

Keywords: MarSCoDe; Tianwen-1; Laser-Induced Breakdown Spectroscopy; wavelength calibration; spectral drift correction

1. Introduction

After the first Laser-Induced Breakdown Spectroscopy (LIBS) was used in an extraterrestrial environment in 2012, the ChemCam of NASA's Curiosity rover was used to investigate the Martian geochemistry [1]. In addition, as a subsequent instrument, the SuperCam of the Perseverance rover, also with LIBS, landed on 18 February 2021 [2]. In China's first Mars exploration Tianwen-1 mission, the lander taking the Zhurong rover successfully landed in the southern part of the Martian Utopian plain on 15 May 2021. As one of the six scientific payloads, the Mars Surface Composition Detector (MarSCoDe) instrument uses LIBS and Short-Wave Infrared (SWIR) spectroscopy to perform he in situ detection of the Martian surface minerals, rocks and soils [3].

LIBS technology can make use of the wavelength and intensity of the characteristic lines of elements in the laser-induced plasma spectrum produced by the ablation of samples

to analyze the chemical composition of the target qualitatively and quantitatively and determine the element concentration in the sample. It is necessary to accurately identify the wavelength position of the emission lines for each element in the spectrum. The spectral line of the LIBS spectrum is not a strict geometric line. The experimental results show that these spectral lines have certain shapes, such as the Doppler broadening, the Lorentz broadening, the self-absorption broadening, Stark broadening and so on [4]. These broadening mechanisms make the spectral peaks follow Gaussian distribution or Lorentz distribution. There may be overlap between different spectral peaks, which affects our judgment of the intensity of the spectral peaks. Among them, Stark broadening not only broadens the spectral line, but also leads to the shift of the peak position [5]. The Stark broadening of the Fe I 538.34 nm emission line can be 0.01–0.06 nm for an electron density between $(4–15) \times 10^{16}$ cm^{-3} [6]. This affects the identification of elements. In addition, the change in environment or the status of the instrument also cause the position of the spectral lines to drift, which greatly reduces the accuracy of the spectral determination, especially in the extraterrestrial LIBS system. Therefore, we need to adopt suitable data-processing methods to correct the wavelength of the LIBS spectrum, improve the accuracy of the position of the characteristic spectral lines of elements, and help to distinguish the emission lines that may be overlapped.

For LIBS in the Mars environment, the main influence factor of the wavelength uncertainty comes from the environmental difference between the extraterrestrial and the Earth. The change in pressure leads to changes in the intensity of the spectral lines. From low pressure to high pressure, the intensity of the spectral lines increases at first and then decreases [7–9]. The change in temperature interferes with the structure of the spectrometer, thus affecting the accuracy of spectral measurement [10]. The changes in temperature and atmosphere between Mars and Earth make it possible to change the position and intensity of the characteristic spectral lines of the elements. The maximum expected drift of the ChemCam spectrometer is about three channels for a ~20 °C operational temperature range. When the temperature changes greatly, it produces a larger offset [11]. The average surface temperature of the Utopian plain can change from 180 K to 240 K in a year. The temperature varies widely and is much lower than the ambient temperature of the ground laboratory. The huge environmental differences make it difficult to directly use the data model established by the laboratory to analyze the in situ exploration data on Mars. The mast unit of the ChemCam is wrapped in a protective cover to ensure that it can run in the range of −40–35 °C [12], greatly reducing the interference of the Martian ambient temperature on the instrument. The mast unit of the SuperCam has independent heaters that enable it to work at temperatures above −40 °C [13]. The Zhurong rover is powered by solar energy and does not have enough power to control the temperature of the MarSCoDe. Therefore, compared with the ChemCam and SuperCam, the MarSCoDe has to go through a more severe test of the Martian environment and adapt to the low temperature on the Martian surface. This may increase the uncertainty of the spectral wavelengths. A lot of research has been carried out to compensate the spectral wavelength drift. Carter et al., proposed a guideline of how to effectively use the polynomials commonly used in spectrometer correction software to convert the number of pixels into wavelength or wavenumber [14]. Holy analyzed the main reason for spectrometer drift and optimized the calibration equation [15]. Asimellis et al., proposed a technique of wavelength calibration based on the inverse numerical solution of the grating dispersion function, which can be used in LIBS and other spectral analyses [16]. Song et al., proposed an efficient and accurate automatic wavelength correction scheme, which improves the calibration accuracy [17]. With respect to correcting the influence of extraterrestrial environment changes on the LIBS spectrum, Wiens et al., used a partial matched filtering technique to calibrate the spectra of the ChemCam to the vacuum wavelengths in the National Institute of Standards and Technology (NIST) LIBS database and correct the wavelength drift [11]. Anderson et al., adopted an optimized ChemCam spectral calibration approach to calibrate the wavelength of the SuperCam's on-board spectrum. In addition to Ti, they also used two additional

targets, one of which is a mixture of ilmenite and hematite, and the other one is a mixture of clinozoisite quartz and orthoclase [18]. Xu et al., studied the temperature-dependent trend of LIBS spectra collected by the MarSCoDe at different temperatures [19]. They selected a certain number of characteristic peaks in each of the three channels of the LIBS spectrometer. With the change in temperature, the pixel drift of each characteristic peak is roughly equal in the same channel. Wan et al., proposed an elastic particle swarm optimization (PSO) approach to fulfill the on-board spectrum calibration of the MarSCoDe [20]. Through the iteration of the particle swarm, the corresponding relationship between wavelengths and pixels is optimized. However, there may be two cases during the instrument launching and landing: (a) the initial wavelength calibration relationship (calibrated on the ground) can still apply to the on-board LIBS measurement, and there is just global drift for each of the three channels; and (b) the initial wavelength calibration relationship is changed, and a new on-board calibration is needed to find the current relationship. In addition, their performance needs further verification.

In this project, two spectral drift correction methods on the MarSCoDe LIBS are presented to deal with the two cases, respectively, and the initial LIBS spectra on the calibration target are conducted and compared. With respect to case (a), a spectrum matching based on the global iterative registration (MGR) approach is presented to identify the amount of spectral drift for each channel and correct the number of pixels, and then calculate the wavelength by the initial relationship. With respect to case (b), a PSO algorithm is verified to build the new relationship and then convert each pixel to the corresponding wavelength. Firstly, the main situation of the MarSCoDe and experimental data set are introduced. Secondly, the spectral calibration method of the LIBS spectrometer is presented. The MGR correction method is proposed for case (a) and the PSO algorithm is described for case (b). Thirdly, the spectral drift correction is carried out by a Ti-alloy calibration sample in the early detection schemes, and the internal accord accuracy is evaluated, while the calibration parameter is also conducted on another eleven calibration samples, and the external accord accuracy is evaluated. Finally, some qualitative and quantitative analysis are compared and discussed.

2. Data Set

2.1. Previous Work Brief

The Zhurong rover left the Tianwen-1 lander and began to inspect and explore on 22 May 2021. As the main payload on-board the rover, the MarSCoDe is an instrument suite and has been described in detail in Xu et al. [19], which takes LIBS to provide an active spectroscopy over 240–850 nm, with a stand-off distance of 1.6~7 m. 1064 nm laser pulses, with the energy of about 23 mJ, at frequency of 1–3 Hz fire the sample. The LIBS spectra within the three channels were recorded using 1800 pixels of the three CCDs, and the spectrum ranges covered by channel 1 (CH-1), channel 2 (CH-2) and channel 3 (CH-3) were 240–340 nm, 340–540 nm and 540–850 nm, respectively. A set of 12 LIBS calibration samples (including Ti-alloy, norite, andesite, basalt, montmorillonite, nontronite, olivine, hypersthene, K-feldspar, gypsum, dolomite and apatite) is mounted on the antenna mast at the rear deck of the rover and about ~1.7 m from a two-dimensional (2D) pointing mirror. Prior to the launch, we calibrated the relationship between the pixels and the wavelength using four standard lamps (including Mercury–Argon, Zinc, Cadmium and Neon), and tested the amount of spectral drift at different temperatures [19]. The main components in the calibration samples were also analyzed by X-ray fluorescence, where the main elements contain Ti, Al, Si, Fe, Mn, Mg, Ca, Na, K, O, P and S, etc.

The brief workflow of the MarSCoDe LIBS in situ detection is to point the laser to the calibration sample through the 2D pointing mirror for the on-board calibration, and then point to the scientific target for the in situ detection. LIBS measurements for each scientific target or calibration sample include 60 consecutive laser shots at frequency of 3 Hz, with an integration of 1 ms and without delay after the laser shot; another 180 passive spectra without laser shots were collected with identical exposure settings and there was a dark

background for each observation. Up to 21 February 2022, a total of 89 LIBS spectra on Level 2B were first released, including 51 spectra of calibration samples and 38 spectra of scientific targets.

2.2. Data Source

In each exploration scheme, the Ti-alloy is first measured and provides on-board wavelength calibration, and then two or three other calibration samples are selected to assess the real-time instrument status, before the scientific detection. We assume that the drift of the spectrum collected by MarSCoDe LIBS in one working cycle is the same. We calibrated the LIBS spectra of each calibration sample collected in the extraterrestrial environment for the first time. A total of 17 spectra were selected from the published on-board calibration data, including six spectra of Ti-alloy and 11 spectra of another eleven samples. The parameters of the LIBS data, collection time and sample name are listed in Table 1. The pressure and temperature come from the data of the Mars Climate Station on the Zhurong rover. Except for the Ti-alloy and norite samples, each spectrum is the first data of these samples measured by the MarSCoDe on Mars. According to the spectra of the calibration samples collected at different times, we selected six Ti-alloy spectra for correction. The abnormality and poor quality of the first norite LIBS spectrum may reduce the accuracy of the qualitative analysis, so we use the second scheme data of norite for the drift correction calculation.

Table 1. On-board LIBS spectral information for drift correction. CAL indicates that the sample is a calibration target.

Martian Day	UTC Time	Data Type	Target No.	Target Name	Pressure (Pa)	Temperature (°C)
Sol 41	2021-06-25T03:15:49	CAL	LC-008	Ti-alloy	825.46	−6.98
Sol 41	2021-06-25T03:17:15	CAL	LC-005	Norite	825.46	−6.98
Sol 41	2021-06-25T03:18:37	CAL	LC-003	Andesite	825.46	−6.98
Sol 43	2021-06-26T23:26:17	CAL	LC-008	Ti-alloy	833.07	−27.53
Sol 43	2021-06-26T23:27:43	CAL	LC-011	Basalt	833.07	−27.53
Sol 45	2021-06-29T07:05:03	CAL	LC-008	Ti-alloy	826.47	−11.28
Sol 45	2021-06-29T07:06:29	CAL	LC-010	Olivine	826.47	−11.28
Sol 45	2021-06-29T07:07:51	CAL	LC-009	Montmorillonite	826.47	−11.28
Sol 47	2021-07-01T02:03:37	CAL	LC-008	Ti-alloy	830.68	−30.41
Sol 47	2021-07-01T02:05:03	CAL	LC-012	K-feldspar	830.68	−30.41
Sol 47	2021-07-01T02:06:25	CAL	LC-001	Gypsum	830.68	−30.41
Sol 58	2021-07-12T08:45:41	CAL	LC-008	Ti-alloy	824.74	−30.78
Sol 58	2021-07-12T08:47:07	CAL	LC-007	Dolomite	824.74	−30.78
Sol 58	2021-07-12T08:48:29	CAL	LC-004	Nontronite	824.74	−30.78
Sol 65	2021-07-19T16:15:56	CAL	LC-008	Ti-alloy	814.315	−12.44
Sol 65	2021-07-19T16:17:22	CAL	LC-002	Hypersthene	814.315	−12.44
Sol 65	2021-07-19T16:18:44	CAL	LC-006	Apatite	814.315	−12.44

The spectrum relevance to LIBS in the Atomic Spectra Database (ASD) of NIST [21] is used as the standard to correct the on-board data. The ASD contains data for radiative transitions and energy levels in atoms and atomic ions. For a given electron temperature and electron density, the level populations and radiative transition probabilities are calculated, and then the spectrum is determined. The default values of electron temperature and electron density are 1eV and 10^{17} cm^{-3}. The parameters are roughly set on the basis of the plasma temperature and density of the ChemCam spectrum for the validation of the proposed method [22]. We download the emission lines of nine main elements (such as Ti,

Al, Si, Fe, Mg, Ca, Na, K and O), two minor elements (Mn, P) and one trace element (S) in the 220 nm–870 nm range under vacuum conditions from the NIST database website as the standard wavelength. Some of the main characteristic peaks used in the spectral calibration approach are shown in Tables A1 and A2 in Appendix A. We do not use the wavelength values in air in the database because the Martian pressure is about 700 Pa, which is closer to a vacuum. According to the Ritz principle, the wavenumber of an emitted or absorbed photon is equal to the difference between the upper and lower energy levels. The value of wavelengths in vacuum is equal to the inverse of wavenumber, where wavenumber is in cm^{-1} and wavelength is in nm.

In addition, the MGR algorithm proposed in this paper selects a reference spectrum to identify the wavelength drift between the on-board spectrum and this reference spectrum, to improve the efficiency and accuracy of wavelength correction. The reference spectrum is the LIBS spectrum of the Ti-alloy sample collected by the MarSCoDe in a simulated Martian environment before the launching. The Ti-alloy is placed in a vacuum chamber filled with CO_2 at a pressure of 874 Pa and a temperature of 24 °C. The MarSCoDe was exposed to the laboratory environment and the spectrum was collected at a distance of 1.7 m from the sample.

3. Methodology

The conversion relationship between responded pixel and spectral wavelength is assumed, and it was determined by the spectral calibration with four standard lamps prior to launch. There are some spectral drifts with the temperature change, due to the limited temperature control of the equipment. There are two main cases: (a) the initial wavelength calibration relationship (calibrated on the ground) can still apply to the on-board LIBS measurement, which means there is just global drift for each of the three channels; and (b) the initial wavelength calibration relationship is changed through impact during launch or landing and the long-term flight environment.

3.1. The Principle of Wavelength Calibration

Spectral calibration of the spectrometer is the premise and basis for the quantitative analysis of LIBS. With respect to the wavelength calibration on the MarSCoDe LIBS spectrometer, the standard lamp with more characteristic spectral lines is used as the input signal for the spectrometer to mark the pixel position corresponding to the specific spectral line, and then the polynomial function fits the relationship between the response pixel and a given wavelength, so as to establish the conversion relationship between all the pixels and the wavelength. The appropriate characteristic spectral lines are selected so that they can evenly cover the wavelength range of each channel. Suppose the wavelength of the characteristic spectral line is $\lambda = [\lambda_1, \lambda_2, \lambda_3, \ldots, \lambda_n]$, n denotes the number of characteristic lines, and the corresponding pixel index is $P = [p_1, p_2, p_3, \ldots, p_n]$, then the pixel–wavelength relationship can be expressed as

$$\lambda_n = a_0 + a_1 p_1 + a_2 p_2^2 + \ldots + a_j p_n^j \tag{1}$$

where a_j is the coefficient of the polynomial and j is the order of the polynomial. In the experiment, the quadratic function is used in the three channels to describe the relationship between pixel and wavelength. The calibration coefficients in the three channels of the spectrometer are calculated in Table 2 [19].

Table 2. The wavelength calibration coefficient in the three channels of the spectrometer (referenced from the Level 2B data).

Channel	a_0	a_1	a_2
CH-1	223.4616	0.0682	-8.1556×10^{-7}
CH-2	76.7535	0.1386	-1.1347×10^{-6}
CH-3	−257.6474	0.2225	-2.1432×10^{-6}

3.2. Spectral Drift Corrected by MGR Algorithm

When the MarSCoDe works, the average temperature on Mars is $-16\ {}^\circ$C, the pressure is about 840 Pa, and the gas is mainly composed of CO_2, including a small amount of N_2, Ar and so on [23]. With respect to case (a), the wavelength of the characteristic lines of elements collected in the Martian environment drift to a certain extent compared with the corresponding lines in the NIST database. In addition, the relative intensity and number of characteristic lines also change, which makes it more difficult to correct the drift of on-board data.

The wavelength drift caused by temperature shows the law of overall drift in the same channel, as demonstrated in Xu et al. [19]. Based on this assumption, we propose the MGR approach for the wavelength correction of MarSCoDe LIBS. The drift situation within the channel is determined by the amount of responded pixel drift of the characteristic spectral lines, and then the drift correction of the LIBS measurements can be obtained. The drift correction of the LIBS measurements can be realized by adding a correction to the responded pixel. Through several iterations of spectral matching, the correction pixel with an optimal matching degree is selected.

In order to correct the spectral drift more conveniently and accurately, the reference spectrum is used as the bridge between the standard spectrum and the on-board data. Firstly, the drift between the reference spectrum and the standard spectrum is calculated, denoted as Δp_1. The reference spectra were qualitatively analyzed, and the corresponding standard spectral wavelength values of the main characteristic peaks were determined. The approximate pixel drift value of the reference spectrum can be obtained according to the sampling interval wavelength, and the reference spectrum can be moved within a certain range. At each drift, the root-mean-square error (RMSE) of the matching peak between the reference spectrum and the standard spectrum was calculated and used as the optimization standard. The correction pixel with an optimal matching degree is Δp_2. Secondly, the drift between the reference spectrum and the on-board spectrum is calculated, denoted as Δp_2. Like the calculation process of Δp_1, the reference spectrum is matched with the on-board Ti-alloy spectrum, and the approximate pixel drift is calculated. The on-board spectrum is moved within a certain range, and the correction pixel is selected with the optimal matching degree, namely Δp_2. The formula of RMSE is

$$\text{RMSE} = \sqrt{\frac{1}{n}\sum_{i=1}^{n}(\lambda_{1i} - \lambda_{2i})^2} \qquad (2)$$

where λ_{1i} and λ_{2i} represent the wavelength values of the matched peaks of the two spectra to be compared, respectively, and n indicates the number of matching peaks. Finally, through the data transmission of the reference spectrum, the on-board data can be associated with the NIST database. The correction formula for wavelength drift is

$$\lambda = a_0 + a_1(p + \Delta p_1 + \Delta p_2) + a_2(p + \Delta p_1 + \Delta p_2)^2 \qquad (3)$$

3.3. Spectral Drift Corrected by Particle Swarm Optimization (PSO) Algorithm

With respect to case (b), the PSO algorithm test in Wan et al. [20] is used here to conduct the on-board calibration of MarSCoDe LIBS. The PSO algorithm is a bionic swarm intelligence algorithm proposed by American scholars Kennedy and Eberhart in 1995, inspired by the foraging behavior of birds [24]. It completes the update and optimization by searching the individual optimal solution of the particle and the global optimal solution of the particle population. For the spectrum set in each channel, a particle swarm that contains several particles is set up. Each particle moves freely in the solution space. The position of the particle represents the coefficient in Formula (1). Bringing it into Formula (1), the new spectral coordinates are obtained and recorded as the particle wavelength set (PWS). The RMSEs of the matching peaks between the PWS and the standard spectrum are calculated.

After many iterations, the particle position with the minimum error, that is, the optimal wavelength calibration coefficient, is calculated.

3.4. Comparison and Evaluation

Based on the wavelength values in the NIST database, the on-board data are corrected by MGR and PSO. In order to verify the accuracy and reliability of the calibration approach, the calibration results are evaluated from two aspects: internal accord accuracy and external accord accuracy. In the internal accord accuracy, the corrected parameter of the Ti-alloy spectrum is first determined by the correction approach and referencing the NIST wavelength, and then used for the drift correction of this spectrum; the wavelength accuracy of the characteristic lines in the corrected spectrum is compared to the NIST database. In the external accord accuracy, the corrected parameter is used to correct the spectrum of the other 11 calibration samples, and then the wavelength accuracy of the characteristic lines is compared to the elemental spectral lines in the samples from the NIST database. Referencing the NIST database, the indicators of absolute mean error (AME) and RMSE on the corrected spectra are used to quantitatively analyze the correction accuracy.

4. Results and Discussion

4.1. The Results of MGR Algorithm

In the calculation of Δp_1, the reference spectrum is preprocessed, including dark background subtraction, noise filtering, cubic spline interpolation fitting and min–max normalization. According to the initial wavelength calibration coefficient in Table 2, the initial wavelength sampling intervals of the three channels are 0.0667 nm, 0.1324 nm and 0.2033 nm, respectively. Figure 1 shows the variation in RMSE obtained by moving the reference spectrum each time. It can be obviously observed that the RMSE shows a parabolic trend with the change in the number of corrected pixels. The abscissa corresponding to the minimum RMSE is the drift of the reference spectrum with respect to the standard spectrum. The spectral drift correction amounts of the three channels are 1.40, 1.39 and 0.45 pixels, respectively, with an RMSE of 0.0258, 0.0362 and 0.0550 nm, respectively.
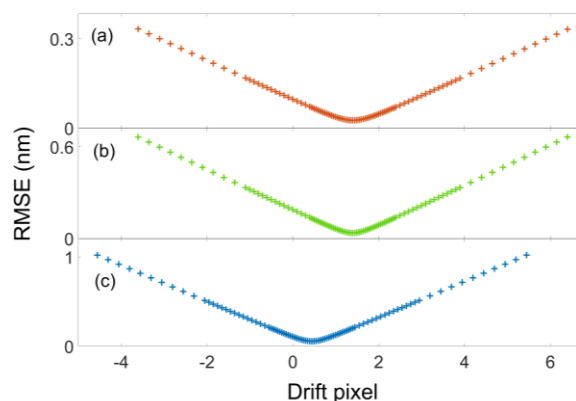
Figure 1. RMSE of reference spectrum calibrated with different drift amounts. RMSE of the corrected reference spectrum varies with the number of drifted pixels. (**a**–**c**) represent the change law of RMSE in the CH-1, CH-2 and CH-3, respectively.

In the calculation of Δp_2, the on-board spectra need to be preprocessed in the same way as the reference spectra. The published on-board data have been subject to dark background subtraction and radiation calibration, so we only need to perform cubic spline interpolation fitting and min–max normalization on the on-board spectrum. The spectra of the Ti-alloy collected by MarSCoDe LIBS on different Martian days are compared with the reference spectrum after the same processing. Taking the Ti-alloy spectrum collected on 25 June 2021 as an example, Figure 2 shows the changes in the spectrum before and after correction and the change diagram of the RMSE. The length of both the reference

spectrum and the on-board spectrum is 5400 pixels, so the position of the peak position in calculation is the pixel rather than the wavelength when the peaks are matched. The RMSE is also measured in pixels. As can be seen from Figure 2, the matching peaks in each channel are distributed as evenly as possible. The corrected spectrum is in good agreement with the reference spectrum. The change in RMSE is also a parabola trend. The position of the minimum RMSE is the best correction amount. Table 3 shows the Δp_2 and RMSE of six Ti-alloy spectra. The mean RMSE for the three channels is 0.138, 0.119 and 0.163 pixels, respectively. The RMSEs of all three channels are better than 0.2 pixels. The corrections of the Ti-alloy spectra collected at different times are different. This has to do with the different environment and instrument states at each probe. The drift of the first channel and the second channel is small, and the drift of the third channel is the largest.
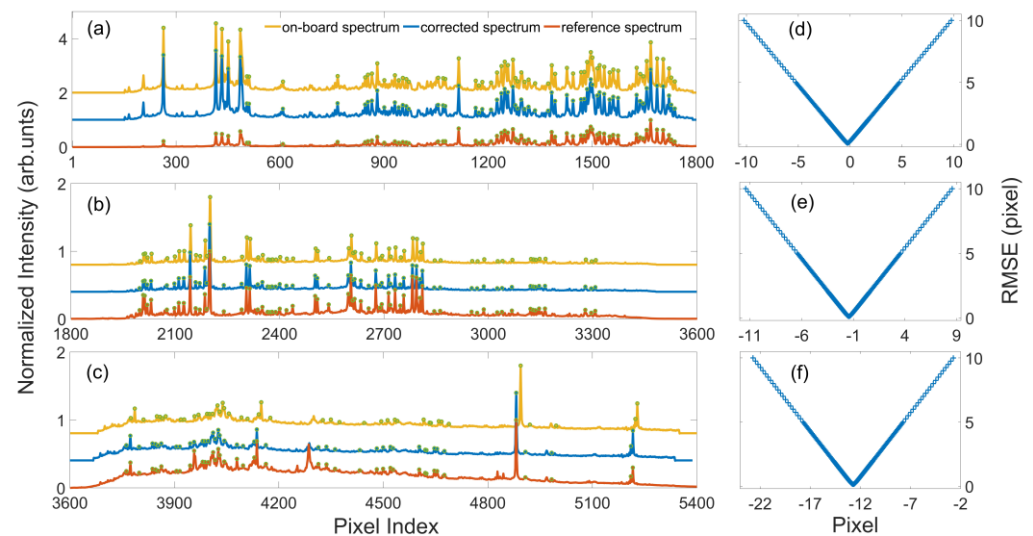
Figure 2. On-board spectra before and after drift correction using the reference spectrum as a reference. The reference spectrum is the spectrum of the Ti-alloy collected by the MarSCoDe in a simulated Martian environment before launch. (**a**–**c**) show the three channels' spectra of the on-board Ti-alloy before and after Δp_2 correction and corresponding reference spectrum. The position of the matching peaks is circled. The spectrum intensity is offset for clarity. (**d**–**f**) show the RMSE change diagram of the on-board spectrum during the translation iterative. The spectrum was collected by the MarSCoDe on 25 June 2021.

Table 3. Δp_2 and RMSE of Ti-alloy spectra collected by the MarSCoDe at different times.

Martian Day	CH-1 (Pixel)	RMSE (Pixel)	CH-2 (Pixel)	RMSE (Pixel)	CH-3 (Pixel)	RMSE (Pixel)
Sol 41	−0.24	0.106	−1.43	0.119	−12.72	0.147
Sol 43	−3.58	0.158	−3.45	0.116	−16.65	0.173
Sol 45	−0.34	0.108	−1.57	0.117	−12.89	0.139
Sol 47	−3.67	0.156	−3.51	0.114	−16.78	0.170
Sol 58	−4.04	0.158	−3.91	0.119	−16.97	0.170
Sol 65	−1.52	0.144	−2.25	0.131	−15.48	0.176
Mean	—	0.138	—	0.119	—	0.163

4.2. The Results of PSO Algorithm

We use the PSO algorithm to correct the drift of on-board Ti-alloy spectra and obtain the new relationship between the responded pixel and wavelength. The on-board spectrum is performed by cubic spline interpolation fitting and min–max normalization before correction. The wavelength calibration coefficient after correction is shown in Table 4. The correction coefficients of the spectra collected at different times are different. Taking the

Ti-alloy spectrum collected on 25 June 2021 as an example, Figure 3 shows the change in RMSE with the number of iterations during the iteration process. In the previous iterative calculation, the matching error decreased rapidly. With the increase in the number of iterations, the rate of error reduction becomes slower and slower, which indicates that it is close to the optimal solution.

Table 4. The wavelength calibration coefficients of different Ti-alloy spectra corrected by PSO.

| Martian Day	Channel	a_0	a_1	a_2
Sol 41	CH-1	223.5197	0.0682	-8.3685×10^{-7}
	CH-2	77.0873	0.1383	-1.0898×10^{-6}
	CH-3	-257.6925	0.2212	-1.9791×10^{-6}
Sol 43	CH-1	223.3008	0.06822	-8.3661×10^{-7}
	CH-2	76.8582	0.1383	-1.0852×10^{-6}
	CH-3	-257.9439	0.2209	-1.9492×10^{-6}
Sol 45	CH-1	223.5126	0.0682	-8.3584×10^{-7}
	CH-2	77.0761	0.1383	-1.0889×10^{-6}
	CH-3	-255.2952	0.2201	-1.8639×10^{-6}
Sol 47	CH-1	223.2976	0.0682	-8.3146×10^{-7}
	CH-2	76.8782	0.1382	-1.0789×10^{-6}
	CH-3	-260.3601	0.2221	-2.0919×10^{-6}
Sol 58	CH-1	223.2742	0.0682	-8.3067×10^{-7}
	CH-2	76.8563	0.1382	-1.0751×10^{-6}
	CH-3	-258.1259	0.2210	-1.9634×10^{-6}
Sol 65	CH-1	223.4329	0.0682	-8.3679×10^{-7}
	CH-2	76.9265	0.1383	-1.0990×10^{-6}
	CH-3	-253.5951	0.2191	-1.7539×10^{-6}
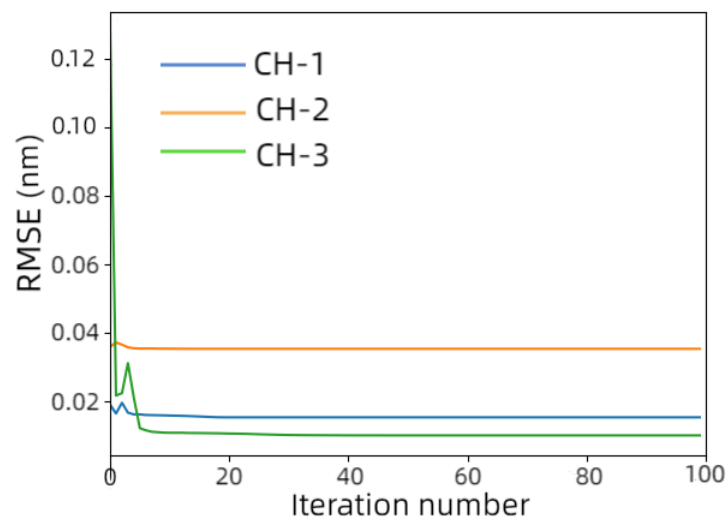
Figure 3. The change trend of RMSE with the number of iterations in the iteration process of the PSO algorithm. Blue, orange and green represent the spectra of the first, second and third channels, respectively.

4.3. Comparison of the Two Methods

4.3.1. Internal Accord Accuracy

Referencing the NIST database, the total wavelength drift of the on-board Ti-alloy spectrum obtained by the MGR method is shown in Table 5. The drift of the spectrum is different at different times. For example, in the spectrum set of CH-1, the minimum drift is only 0.24 pixels, and the maximum drift is 4.04 pixels; in the spectrum set of CH-2, the minimum drift is only 1.43 pixels, and the maximum drift is 3.91 pixels; and in the CH-3, the minimum drift is only 12.72 pixels, and the maximum drift is 12.97 pixels. This is related to the changes in environment on Mars. As can be seen from Table 1, the temperature and air pressure are different every day. We carry Δp_1 and Δp_2 into Equation (3) to obtain the corrected on-board spectral wavelength. Table 6 shows the AME and RMSE of two different spectral wavelength drift correction approaches. For the accuracy of MGR, the mean errors in the first, second and third channel is 0.016 nm, 0.022 nm and 0.040 nm, and the RMSE is 0.020 nm, 0.030 nm and 0.050 nm, respectively. According to the sampling interval wavelength value corresponding to each pixel, the mean error is 0.232 pixels, 0.166 pixels and 0.195 pixels, and the RMSE is 0.292 pixels, 0.223 pixels and 0.247 pixel, respectively. Furthermore, the maximum error is 29.2% of the pixel (on the RMSE of CH-1), so that the overall accuracy is better than one-third of the pixel. For the accuracy of the PSO, the mean error in the first, second and third channel is 0.017 nm, 0.031 nm and 0.021 nm, and the RMSE is 0.023 nm, 0.039 nm and 0.026 nm, respectively. According to the sampling interval wavelength value corresponding to each pixel, the mean error is 0.255 pixels, 0.230 pixels and 0.104 pixels, and the RMSE is 0.342 pixels, 0.291 pixels and 0.104 pixels, respectively. In addition, the maximum error is 34.2% of the pixel (on the RMSE of CH-1), so that the overall accuracy is nearly one-third of the pixel. The errors may come from the limitation of spectral resolution, which makes it impossible for us to accurately determine the position of the spectral peaks. In addition, Stark broadening is also one of the important factors affecting the correction effect. The collision of atoms with ions and electrons shifts the position of the spectral peak. Since the spectral resolution of the three channels of the MarSCoDe is nearly 0.19 nm, 0.31 nm and 0.45 nm, respectively, which is much higher than the shift range of spectral lines caused by Stark broadening, in this study, we ignore the influence of spectral line drift caused by Stark broadening and focus on the spectral drift caused by environmental changes. We do not analyze the Stark shift of the spectrum, which may be one of the sources of the final error. It should also be noted that, in this paper, we assume that the MarSCoDe LIBS spectrum satisfies the local thermal equilibrium, which is consistent with the data in the NIST database. However, we do not have strong data to support this hypothesis. This may also be one of the sources of error. From the results of the RMSE, the effect of the MGR method is better than that of the PSO algorithm in the first and second channel, and slightly inferior to the PSO method in the third channel. This may be due to the low resolution of the third channel spectrometer. The uncertainty of the position of the characteristic peaks makes the fitting calibration relationship more accurate. In Table 5, the number of matching peaks selected by the MGR and PSO methods for spectral correction is counted. Due to the change in environment, the intensity value of the Ti-alloy spectrum collected at different times changes, and the number of characteristic peaks is also different. As many characteristic peaks as possible were selected in each channel for spectral correction and accuracy evaluation. Taking the Ti-alloy spectrum collected on 12 July 2021 as an example, Figure 4 shows the spectra before and after wavelength drift correction by the MGR and PSO methods. As can be seen from the figure, the number of characteristic lines in the third channel is much smaller than that in the first and second channels. After correction, the two methods can solve the problem of spectral drift well.

Table 5. Total drift amount and RMSE by MGR method of Ti-alloy spectra and the number of characteristic peaks used in the spectral correction of each channel.

Martian Day	CH-1		CH-2		CH-3	
	Drift Amount (Pixel)	Number of Characteristic Lines	Drift Amount (Pixel)	Number of Characteristic Lines	Drift Amount (Pixel)	Number of Characteristic Lines
Sol 41	−0.24	68	−1.43	50	−12.72	23
Sol 43	−3.58	68	−3.45	29	−16.65	24
Sol 45	−0.34	70	−1.57	53	−12.89	27
Sol 47	−3.67	78	−3.51	51	−16.78	42
Sol 58	−4.04	75	−3.91	50	−16.97	45
Sol 65	−1.52	69	−2.25	54	−15.48	24

Table 6. The absolute mean error (AME) and RMSE of the corrected Ti-alloy spectrum. Two methods of MGR and PSO are used to correct the on-board spectrum.

Martian Day	Method	CH-1 (nm)		CH-2 (nm)		CH-3 (nm)	
		AME	RMSE	AME	RMSE	AME	RMSE
Sol 41	MGR	0.015	0.019	0.021	0.029	0.031	0.040
	PSO	0.017	0.024	0.029	0.038	0.016	0.021
Sol 43	MGR	0.015	0.019	0.021	0.029	0.040	0.050
	PSO	0.017	0.024	0.031	0.038	0.023	0.029
Sol 45	MGR	0.015	0.019	0.023	0.031	0.040	0.051
	PSO	0.018	0.024	0.030	0.039	0.025	0.030
Sol 47	MGR	0.017	0.021	0.023	0.030	0.045	0.057
	PSO	0.019	0.025	0.032	0.040	0.030	0.035
Sol 58	MGR	0.016	0.020	0.023	0.030	0.047	0.058
	PSO	0.018	0.025	0.033	0.041	0.024	0.029
Sol 65	MGR	0.015	0.019	0.021	0.028	0.035	0.045
	PSO	0.013	0.015	0.028	0.035	0.009	0.010
Mean	MGR	0.016	0.020	0.022	0.030	0.040	0.050
	PSO	0.017	0.023	0.031	0.039	0.021	0.026

4.3.2. External Accord Accuracy

The correction amount or correction coefficient obtained from the Ti-alloy spectrum is carried into other samples' spectra to realize the drift correction. We used MGR and PSO approaches to correct the spectra of another 11 calibration samples and calculated the mean error and RMSE of the matching peaks, as shown in Table 7. For the accuracy of MGR, the mean errors in the first, second and third channel is 0.012 nm, 0.033 nm and 0.040 nm, and the RMSE is 0.015 nm, 0.042 nm and 0.0460 nm, respectively. According to the sampling interval wavelength value corresponding to each pixel, the mean error is 0.183 pixels, 0.253 pixels and 0.195 pixels, and the RMSE is 0.232 pixels, 0.316 pixels and 0.229 pixels, respectively. Furthermore, the maximum error is 31.6% of the pixel (on the RMSE of CH-2), so that the overall accuracy is also better than one-third of the pixel. For the accuracy of the PSO, the mean error in the first, second and third channel is 0.012 nm, 0.040 nm and 0.052 nm, and the RMSE is 0.017 nm, 0.047 nm and 0.066 nm, respectively. According to the sampling interval wavelength value corresponding to each pixel, the mean errors is 0.179 pixels, 0.305 pixels and 0.254 pixels, and the RMSE is 0.251 pixels, 0.357 pixels and 0.326 pixels, respectively. In addition, the maximum error is 35.7% of the pixel (on the RMSE of CH-2), so that the overall accuracy is also nearly one-third of the

pixel. Using RMSE as the evaluation mechanism of the correction approach, the effects of the two methods are almost the same in the first channel. The MGR correction results of individual samples are better, such as Andesite, Montmorillonite and Hypersthene. In the second and third channels, the RMSE of most samples of the MGR algorithm is lower, which shows that its correction effect is better than that of the PSO algorithm. The MGR algorithm is more universal and can be applied to the spectral correction of different samples. Figure 5 shows the on-board spectra of 11 samples before and after wavelength drift correction. The spectra corrected by the two approaches match the NIST database well. Many elements such as Mg, Si, K, Ca, Na, O and C can be identified. Table 7 counts the number of characteristic lines used in the calibration process of the on-board spectra. In some samples, such as gypsum, the number of characteristic peaks is small, but they are uniformly distributed throughout the wavelength range of the spectrometer.
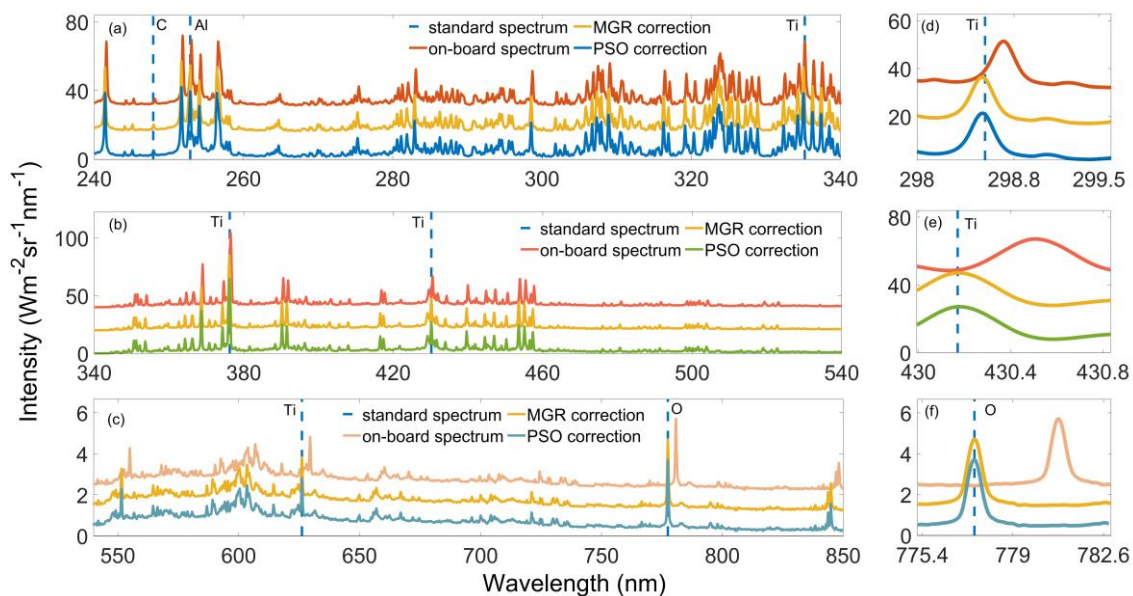
Figure 4. The spectrum of on-board Ti-alloy before and after wavelength drift correction using the MGR approach and PSO approach. (**a**–**c**) represent the spectrum in the CH-1, CH-2 and CH-3, respectively. (**d**–**f**) are the local spectra in the three channels, respectively. The spectrum intensity is offset for clarity.

Table 7. The absolute mean error (AME) and RMSE of corrected on-board spectra and the number of characteristic peaks used in the spectral correction of each channel. In the table, "Number" represents the number of characteristic peaks.

Sample	Correction Method	CH-1			CH-2			CH-3		
		AME (nm)	RMSE (nm)	Number	AME (nm)	RMSE (nm)	Number	AME (nm)	RMSE (nm)	Number
Norite	MGR	0.013	0.018	50	0.038	0.045	15	0.041	0.047	21
	PSO	0.013	0.018	50	0.038	0.045	15	0.040	0.046	21
Andesite	MGR	0.013	0.006	49	0.008	0.044	14	0.037	0.044	17
	PSO	0.012	0.017	49	0.047	0.054	14	0.038	0.047	17
Basalt	MGR	0.013	0.017	43	0.032	0.036	24	0.039	0.048	26
	PSO	0.013	0.018	43	0.040	0.047	24	0.049	0.063	26
Olivine	MGR	0.011	0.016	34	0.035	0.038	18	0.041	0.045	11
	PSO	0.011	0.016	34	0.039	0.046	18	0.040	0.052	11
Montmorillonite	MGR	0.013	0.018	26	0.035	0.039	15	0.044	0.052	18
	PSO	0.014	0.020	26	0.044	0.052	15	0.037	0.053	18
K-feldspar	MGR	0.011	0.015	21	0.042	0.047	29	0.025	0.037	17
	PSO	0.011	0.015	21	0.048	0.055	29	0.085	0.106	17

Table 7. *Cont.*

Sample	Correction Method	CH-1			CH-2			CH-3		
		AME (nm)	RMSE (nm)	Number	AME (nm)	RMSE (nm)	Number	AME (nm)	RMSE (nm)	Number
Gypsum	MGR	0.012	0.017	3	0.038	0.047	5	0.042	0.048	20
	PSO	0.012	0.017	3	0.041	0.049	5	0.069	0.089	20
Dolomite	MGR	0.013	0.017	18	0.027	0.032	13	0.046	0.051	20
	PSO	0.012	0.017	18	0.027	0.032	13	0.052	0.065	20
Nontronite	MGR	0.014	0.018	29	0.044	0.051	13	0.037	0.044	17
	PSO	0.012	0.017	29	0.046	0.053	13	0.037	0.046	17
Hypersthene	MGR	0.011	0.014	35	0.042	0.050	33	0.040	0.046	27
	PSO	0.011	0.015	35	0.044	0.053	33	0.066	0.087	27
Apatite	MGR	0.011	0.014	6	0.027	0.031	9	0.043	0.049	23
	PSO	0.010	0.014	6	0.030	0.034	9	0.055	0.075	23
Mean	MGR	0.012	0.015	—	0.033	0.042	—	0.040	0.046	—
	PSO	0.012	0.017	—	0.040	0.047	—	0.052	0.066	—
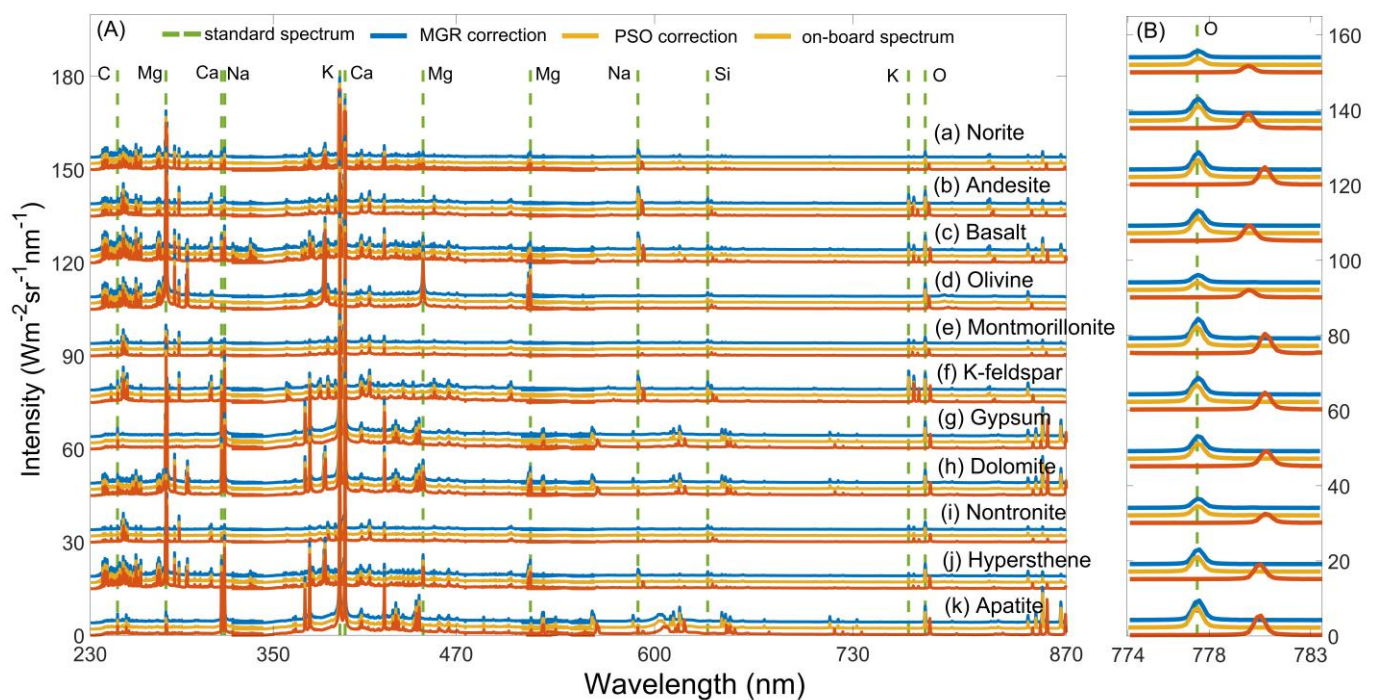
Figure 5. The before and after drift correction spectra of 11 calibration samples obtained by using MGR and PSO. (**A**) is the spectrum in the three channels, and (**B**) is the local spectrum. The vertical dashed lines represent the standard spectra. The blue lines represent the spectra corrected by the MGR method. The orange lines represent the spectra corrected by the PSO method. The red lines represent the uncorrected on-board spectra. The spectrum intensity is offset for clarity.

5. Conclusions

As one extraterrestrial LIBS system, MarSCoDe LIBS also has some spectral drift with the changes in the environmental conditions. Elaborate LIBS spectral calibration is the crucial foundation for realizing accurate qualitative and quantitative analysis, even for sophisticated deep learning based chemometrics [25,26]. There may be two cases during the instrument launch and landing, as well as the long-term operation: (a) the initial wavelength calibration relationship can still apply to the on-board LIBS measurement; and (b) the initial wavelength calibration relationship is changed, and a new on-board calibration is needed to find the current relationship.

In this project, two spectral drift correction approaches of MGR and PSO are presented to deal with the two cases, respectively, and the initial on-board LIBS spectra of the LIBS calibration targets are conducted and compared. Firstly, the main situation of the MarSCoDe and the experimental data are introduced. Secondly, the spectral calibration approach of the LIBS spectrometer is presented. The MGR correction method is proposed for case (a), and the PSO algorithm is described for case (b). Thirdly, the spectral drift correction is carried out using the Ti-alloy calibration sample, and the internal accord accuracy is evaluated, while the calibration parameter is also conducted on other calibration samples, and the external accord accuracy is evaluated. Finally, some qualitative and quantitative analyses are estimated with a comparison to the NIST database. The experimental results show that the proposed approach can effectively correct the drift of the on-board LIBS spectrum, and the RMSE of the internal accord accuracy for the three channels is about 0.292, 0.223 and 0.247 pixels, respectively, compared with the corrected spectrum and the NIST database, and the RMSE of the external accord accuracy is about 0.232, 0.316 and 0.229 pixels, respectively. The overall accuracy of the three channels is better than one-third of sampling interval. Compared with the PSO method, MGR has a better correction effect in the first and second channels. The correction effect of MGR in the third channel is worse, which may be caused by the low spectral resolution in the third channel. When the calibration model obtained from the Ti-alloy spectrum is tested in the spectra of other calibration samples, the MGR method performed better than the PSO method in the three channels. The maximum internal accord accuracy errors of the MGR and PSO methods are about 29.2% and 34.2% of pixels, respectively (on the RMSE of CH-1). The maximum external accord accuracy errors of the MGR and PSO methods are about 31.6% and 35.7% of pixels, respectively (on the RMSE of CH-2). The internal and external accord accuracy of MGR is higher.

Author Contributions: Conceptualization, X.L. and L.J.; methodology, X.L. and W.X.; validation, L.J. and Z.C.; resources, X.X. and L.L.; data curation, L.J. and Z.L.; writing—original draft preparation, L.J.; writing—review and editing, X.L.; supervision, R.S. All authors have read and agreed to the published version of the manuscript.

Data Availability Statement: The data are available upon request from the author.

Conflicts of Interest: The authors declare no conflict of interest.

Appendix A

Table A1. The standard wavelength used in spectral calibration with Ti-alloy. E_i and E_k are the upper and lower energy levels of electron transitions, respectively.

Ion	Wavelength (nm)	E_i (cm^{-1})	E_k (cm^{-1})	Ion	Wavelength (nm)	E_i (cm^{-1})	E_k (cm^{-1})
Ti-II	245.1177	12,758.2597	53,554.9903	Ti-II	364.2366	9975.9994	37,430.6814
C-I	247.9310	21,648.0300	61,981.8321	Ti-II	370.7271	12,628.8455	39,602.8645
Ti-II	251.8189	1087.3561	40,798.4333	Ti-II	372.2695	4628.6571	31,490.9177
Al-II	252.7244	95,350.6000	134,919.4000	Ti-II	374.2702	1700.0000	12,758.2597
Al-II	254.0945	106,920.5600	146,276.0000	Ti-II	376.2389	4628.6571	31,207.5111
Ti-II	255.6755	29,734.6206	68,846.6990	Ti-II	381.5663	4628.6571	30,836.4250
Ti-II	256.5168	38,425.9900	77,424.4500	Ti-I	388.3992	16,458.6710	42,205.3770

Table A1. *Cont.*

Ion	Wavelength (nm)	E_i (cm^{-1})	E_k (cm^{-1})	Ion	Wavelength (nm)	E_i (cm^{-1})	E_k (cm^{-1})
Ti-II	264.6862	40,027.2001	77,807.7864	Ti-I	390.2064	170.1328	25,797.5950
Ti-II	269.9246	43,740.7678	80,788.1500	Ti-I	391.5443	386.8740	25,926.7710
Ti-II	273.1650	31,756.6406	68,364.5454	Ti-I	396.3972	0.0000	25,227.2220
Ti-II	274.7355	31,207.5111	67,606.1621	Ti-II	402.9477	15,257.5527	40,074.6707
Ti-II	275.2420	31,490.9177	67,822.5867	Ti-II	405.4966	15,265.7001	39,926.8192
Ti-II	276.5632	8744.3406	44,902.4455	Ti-I	407.9622	8602.3441	33,114.4200
Ti-II	280.5646	29,544.4540	65,186.8680	Ti-I	416.5305	15,108.1110	39,115.9570
Ti-II	281.1126	9975.9994	45,548.9273	Ti-II	417.3080	20,951.7551	44,914.8733
Ti-II	281.8644	29,968.3304	65,446.3822	Ti-I	429.1422	9395.8020	32,698.1022
Ti-I	282.8896	6742.7560	42,092.2360	Ti-I	430.1764	6661.0060	29,907.2860
Ti-II	284.2770	4897.7179	40,074.6707	Ti-II	430.9077	9395.8020	32,602.6265
Ti-II	285.1939	9851.0145	44,914.8733	Ti-I	431.5557	6742.7560	29,914.7370
Ti- II	285.6923	30,240.9396	65,243.6290	Ti-II	433.9134	8710.5675	31,756.6406
Ti-II	286.3160	9975.9994	44,902.4455	Ti-II	436.8880	20,891.7898	43,780.9533
Ti-II	287.8279	8997.7874	43,740.7678	Ti- II	439.6266	8744.3406	31,490.9177
Ti-II	288.4948	9118.2849	43,780.9533	Ti-II	441.8954	9395.8020	32,025.5915
Ti-II	294.2709	31,113.6764	65,095.9741	Ti-II	444.5048	8710.5675	31,207.5111
Ti-II	295.5434	34,748.5062	68,584.4792	Ti-II	445.1731	8744.3406	31,207.5111
Ti-II	301.8062	12,774.8168	45,908.6592	Ti-II	446.9747	9118.2849	31,490.9177
Ti-II	302.4549	34,543.3799	67,606.1621	Ti-II	448.9583	25,192.9650	47,466.7479
Ti-II	303.0610	12,677.1050	45,673.7641	Ti-II	450.2532	8997.7874	31,207.5111
Ti-II	304.7024	43,780.9533	76,599.8564	Ti-I	453.6048	6742.7560	28,788.3800
Ti-II	305.8761	32,767.1961	65,460.1706	Ti- II	455.0897	12,774.8168	34,748.5062
Ti-II	306.7109	94.1142	32,698.1022	Ti- II	456.5037	9851.0145	31,756.6406
Ti-II	307.3352	29,734.6206	62,272.3881	Ti- II	457.3253	12,677.1050	34,543.3799
Ti-II	307.9538	225.7039	32,698.1022	Ti-II	480.6436	16,625.2441	37,430.6814
Ti-II	308.8922	393.4459	32,767.1961	Ti-II	491.2566	25,192.9650	45,548.9273
Ti- II	309.8081	9930.7766	42,208.8232	Ti-I	498.3120	6842.9620	26,910.7090
Ti-II	310.4703	15,257.5527	47,466.7479	Ti-I	499.2458	6742.7560	26,772.9680
Ti-I	311.1574	12,118.3930	44,257.0980	Ti-I	500.0898	6661.0060	26,657.4160
Ti-II	311.8571	9930.7766	41,996.7498	Ti-I	501.5675	6556.8330	26,494.3300
Ti-II	313.1706	94.1142	32,025.5915	Ti-I	503.7868	11,639.8109	31,489.4760
Ti-I	314.4665	16,458.6710	48,262.7050	Ti- II	519.0132	12,758.2597	32,025.5915
Ti-II	315.6582	1087.3561	32,767.1961	Ti- II	522.7994	128,433.4000	147,562.1400
Ti-II	316.2684	983.9157	32,602.6265	Ti- II	542.0274	12,758.2597	31,207.5111
Ti-II	316.9435	1215.8329	32,767.1961	Ti-I	548.2933	19,421.5800	37,659.9920
Ti-II	319.1795	8744.3406	40,074.6707	Ti-I	549.1673	11,776.8120	29,986.1990
Ti-II	320.3460	8710.5675	39,926.8192	Ti-I	551.5875	11,531.7610	29,661.2500
Ti- II	321.9195	12,677.1050	43,740.7678	Ti-I	556.7019	18,037.2130	36,000.1480
Ti-II	322.5168	12,774.8168	43,780.9533	Ti-I	564.5700	18,287.5540	36,000.1480
Ti-II	323.0122	0.0000	30,958.5846	Ti-I	566.4454	20,006.0390	37,659.9920

Table A1. *Cont.*

Ion	Wavelength (nm)	E_i (cm^{-1})	E_k (cm^{-1})	Ion	Wavelength (nm)	E_i (cm^{-1})	E_k (cm^{-1})
Ti-II	323.7053	8710.5675	39,602.8645	Ti-I	567.6986	18,593.9470	36,208.9290
Ti-II	324.2918	0.0000	30,836.4250	Ti-I	576.7926	26,564.4000	43,901.6548
Ti-II	325.3844	225.7039	30,958.5846	Ti-I	578.7584	26,772.9680	44,051.3351
Ti-II	326.2525	15,257.5527	45,908.6592	Ti-I	580.5869	26,910.7090	44,134.6580
Ti-II	327.2591	10,024.8009	40,581.6301	Ti-I	586.8077	8602.3441	25,643.7010
Ti-II	327.9232	9930.7766	40,425.7183	Ti-II	594.1989	65,095.9741	81,924.1270
Ti-II	328.8601	15,265.7001	45,673.7641	Ti-I	595.4809	15,220.3930	32,013.5440
Ti-II	330.9756	1087.3561	31,301.0653	Ti-I	598.0197	1000.0000	15,108.1110
Ti-II	331.6276	9872.8990	40,027.2001	Ti-II	600.4067	65,186.8680	81,842.2440
Ti-II	332.3890	1215.8329	31,301.0653	Al-II	704.4024	91,274.5000	105,470.9300
Ti-II	333.0411	1087.3561	31,113.6764	Ti-I	721.1423	11,776.8120	25,643.7010
Ti-II	333.6150	983.9157	30,958.5846	Ti-I	724.6851	11,639.8109	25,438.9080
Ti-I	334.2836	0.0000	29,914.7370	Ti-I	725.3708	11,531.7610	25,317.8140
Ti-II	335.0365	393.4459	30,240.9396	Ti-II	729.9330	68,584.4792	82,284.3670
Ti-I	336.2178	170.1328	29,912.2860	Ti-II	731.5316	68,331.1599	82,001.1090
Ti- II	337.3762	94.1142	29,734.6206	O-I	777.4083	73,768.2000	86,631.4540
Ti-II	338.4730	0.0000	29,544.4540	O-I	794.9734	101,135.4070	113,714.4440
Ti-II	339.5547	94.1142	29,544.4540	Ti-I	795.1338	12,118.3930	24,694.8920
Ti-II	350.6022	44,914.8733	73,437.2269	Ti-I	798.1010	15,220.3930	27,750.1350
Ti-II	351.1844	15,265.7001	43,740.7678	Ti-I	838.4834	6598.7650	18,525.0590
Ti-II	352.1259	16,515.9359	44,914.8733	Ti-I	842.8823	6661.0060	18,525.0590
Ti-II	353.6418	16,625.2441	44,902.4455	Ti-I	843.7272	6842.9620	18,695.1340
Ti-II	359.7073	4897.7179	32,698.1022	O-I	844.8680	76,794.9780	88,631.1460

Table A2. The standard wavelength used in spectral validation with other calibration samples. E_i and E_k are the upper and lower energy levels of electron transitions, respectively.

Ion	Wavelength (nm)	E_i (cm^{-1})	E_k (cm^{-1})	Ion	Wavelength (nm)	E_i (cm^{-1})	E_k (cm^{-1})
Fe-II	240.5162	862.6118	42,439.8511	Si-I	390.6629	15,394.3700	40,991.8840
Fe-II	240.5617	667.6829	42,237.0575	S-II	393.4378	131,187.1900	156,604.1700
Fe-II	241.1252	862.6118	42,334.8444	K-II	393.5520	201,957.6000	227,367.2000
Na-II	242.4442	331,186.7000	372,433.3000	Al-I	394.5122	0.0000	25,347.7560
Fe-II	242.4881	22,637.1950	63,876.3250	C-I	396.2524	61,981.8321	87,218.2750
Si-I	243.5893	6298.8500	47,351.5540	Al-I	396.2641	112.0610	25,347.7560
Fe-II	244.5256	20,830.5534	61,726.0690	Ca-II	396.9591	0.0000	25,191.5100
Fe-II	244.5847	41,968.0698	82,853.7040	Fe-I	404.6955	11,976.2390	36,686.1760
Fe-II	246.2028	26,055.4120	66,672.3360	K-I	404.8356	0.0000	24,701.3820
C-I	247.9310	21,648.0300	61,981.8321	Si-II	407.7931	79,338.5000	103,860.7400
Fe-II	248.3616	44,784.7859	85,048.6550	Fe-I	407.9505	21,038.9870	45,551.7670
Na-II	249.3900	268,762.9600	308,860.8000	Na-II	408.8747	268,762.9600	293,220.3300
Fe-II	249.9651	21,581.6151	61,587.2050	Al-III	408.9765	178,470.3200	202,921.6000
Si-I	250.7652	77.1150	39,955.0530	Si-II	413.2059	79,355.0200	103,556.0300

Table A2. *Cont.*

Ion	Wavelength (nm)	E_i (cm^{-1})	E_k (cm^{-1})	Ion	Wavelength (nm)	E_i (cm^{-1})	E_k (cm^{-1})
Si-I	251.6870	223.1570	39,955.0530	K-II	418.7412	162,502.7000	186,383.8000
Si-I	251.9960	77.1150	39,760.2850	Ca-I	422.7918	0.0000	23,652.3040
Si-I	252.4867	77.1150	39,683.1630	Al-II	422.8006	121,483.5000	145,135.3100
Si-I	252.9268	223.1570	39,760.2850	Fe-I	422.8617	26,874.5500	50,522.9440
p-I	253.6374	18,748.0100	58,174.3660	C-II	426.8202	145,549.2700	168,978.3400
Fe-II	253.9561	21,430.3564	60,807.2390	Fe-I	427.2962	11,976.2390	35,379.2080
Fe-II	253.9672	21,581.6151	60,956.7810	Ca-I	430.3738	15,315.9430	38,551.5580
Ca-III	254.2262	242,547.1900	281,882.2400	Ca-I	431.9866	15,315.9430	38,464.8080
Fe-II	255.0160	23,031.2829	62,244.5150	Fe-I	432.6978	12,968.5540	36,079.3720
Fe-II	255.0227	22,939.3512	62,151.5540	C-I	435.0190	64,089.8990	87,077.4020
Si-III	255.9963	165,765.0000	204,828.0600	Mg-II	438.5869	80,619.5000	103,420.0000
Fe-II	256.3304	7955.3186	46,967.4751	Fe-I	441.6362	12,968.5540	35,611.6250
Fe-II	256.4244	8391.9554	47,389.8090	Ca-I	443.6202	15,210.0630	37,751.8670
Si-I	256.4446	6298.8500	45,293.6290	Na-II	445.5977	332,841.9300	355,283.7000
Mg-I	257.5713	21,911.1780	60,735.3800	Na-II	445.6481	332,841.9300	355,281.1600
Mg-I	258.6327	21,870.4640	60,535.3400	Mg-II	448.2383	71,490.1900	93,799.7500
Fe-II	258.6649	0.0000	38,660.0537	Na-II	453.0524	342,971.0000	365,043.5000
Fe-II	260.0172	0.0000	38,458.9934	Na-II	455.3050	331,873.9300	353,837.2300
Mg-I	260.7398	21,911.1780	60,263.5830	Si-III	455.3898	153,377.0500	175,336.2600
Fe-II	260.7866	667.6829	39,013.2160	Ca-III	455.4568	339,198.0900	361,154.0700
Na-II	261.2591	293,220.3300	331,496.5100	Si-III	456.9121	153,377.0500	175,263.1000
Fe-II	261.8399	65,580.0650	103,771.3420	Na-II	459.2222	308,860.8000	330,636.7500
Fe-II	262.6450	384.7872	38,458.9934	K-I	464.3175	0.0000	21,536.9880
Fe-II	263.1831	862.6118	38,858.9696	Al-II	464.9911	124,794.1300	146,299.9200
Si-I	263.2066	15,394.3700	53,387.3340	Mg-I	470.4307	35,051.2640	56,308.3810
Fe-II	263.2107	667.6829	38,660.0537	Ca-III	470.4917	323,003.5600	344,257.9200
Fe-II	272.8191	25,428.7893	62,083.1180	C-I	504.3203	64,090.9935	83,919.6632
Fe-II	272.8346	8391.9554	45,044.1916	K-II	505.7657	163,432.1000	183,204.1000
Fe-II	274.0358	7955.3186	44,446.9051	C-I	505.9088	69,744.0521	89,510.4600
Fe-II	274.4008	8846.7837	45,289.8248	Mg-I	516.8761	21,850.4050	41,197.4030
Fe-II	274.4033	42,401.3198	78,844.0310	Mg-I	517.4125	21,870.4640	41,197.4030
Fe-II	274.9994	8680.4706	45,044.1916	Mg-I	518.5048	21,911.1780	41,197.4030
Fe-II	275.0134	8391.9554	44,753.8179	Ca-I	527.1737	20,371.0000	39,340.0800
Na-II	275.0451	332,841.9300	369,199.6000	Ca-I	551.4512	23,652.3040	41,786.2760
Fe-II	275.6551	7955.3186	44,232.5398	Mg-I	552.9940	35,051.2640	53,134.6420
Fe-II	276.8329	42,114.8380	78,237.7090	P-II	558.9852	106,001.2500	123,890.8100
Mg-I	278.0641	21,870.4640	57,833.4000	Ca-I	559.0301	20,371.0000	38,259.1240
Mg-II	279.1600	35,669.3100	71,491.0600	Si-II	569.0396	114,414.5800	131,988.0500
Mg-II	279.6352	0.0000	35,760.8800	Al-III	569.8184	126,164.0500	143,713.5000
Mg-II	279.8823	35,760.8800	71,490.1900	Al-III	572.4318	126,164.0500	143,633.3800
Mg-II	280.3531	0.0000	35,669.3100	Si-III	574.1326	159,069.6100	176,487.1900

Table A2. *Cont.*

Ion	Wavelength (nm)	E_i (cm^{-1})	E_k (cm^{-1})	Ion	Wavelength (nm)	E_i (cm^{-1})	E_k (cm^{-1})
Al-II	281.7014	59,852.0200	95,350.6000	Ca-I	585.9074	23,652.3040	40,719.8470
Mg-I	285.2964	0.0000	35,051.2640	Na-I	589.1583	0.0000	16,973.3662
Si-I	288.2423	6298.8500	40,991.8840	Na-I	589.7558	0.0000	16,956.1703
Mg-II	292.9490	35,669.3100	69,804.9500	C-I	598.2894	64,086.9696	80,801.2889
Mg-II	293.7369	35,760.8800	69,804.9500	S-II	610.3955	114,804.3700	131,187.1900
Mg-I	293.7600	21,850.4050	55,891.8000	Ca-I	610.4412	15,157.9010	31,539.4950
Na-II	298.5061	298,165.4400	331,665.5900	Ca-I	612.3912	15,210.0630	31,539.4950
Fe-I	302.1370	704.0070	33,801.5720	S-II	612.5090	113,461.5400	129,787.8300
Al-I	308.3046	0.0000	32,435.4530	Ca-I	616.3878	15,315.9430	31,539.4950
Si-III	308.7132	142,943.7400	175,336.2600	Ca-I	617.1270	20,371.0000	36,575.1190
Na-II	308.7953	298,165.4400	330,549.3500	Mg-III	624.5745	548,720.7000	564,731.6000
Mg-I	309.3884	21,870.4640	54,192.2940	Si-II	634.8864	65,500.4700	81,251.3200
Mg-I	309.7790	21,911.1780	54,192.2560	Si-II	637.3133	65,500.4700	81,191.3400
Na-II	315.0187	268,762.9600	300,507.1100	Ca-I	644.0855	20,371.0000	35,896.8890
Ca-II	315.9783	25,191.5100	56,839.2500	Ca-I	645.1591	20,335.3600	35,835.4130
Mg-II	316.6795	80,619.5000	112,197.1700	Ca-I	646.4353	20,349.2600	35,818.7130
Na-II	317.9975	299,189.9600	330,636.7500	Ca-I	647.3450	20,371.0000	35,818.7130
Si-III	323.4887	175,263.1000	206,176.0800	Ca-I	649.5576	20,335.3600	35,730.4540
Mg-III	336.2362	534,923.6000	564,664.6000	C-II	657.9869	116,537.6500	131,735.5200
Ca-III	337.3647	242,547.1900	272,188.7000	C-I	658.0586	72,610.7353	87,806.9500
Fe-I	357.1273	22,650.4160	50,651.6320	P-I	671.9256	64,239.5910	79,122.1900
K-II	358.7586	187,527.0000	215,400.9000	Ca-I	671.9536	21,849.6340	36,731.6150
Al-III	360.2954	115,958.5000	143,713.5000	Al-II	704.4024	91,274.5000	105,470.9300
Fe-I	368.7046	23,711.4560	50,833.4380	K-I	766.7009	0.0000	13,042.8960
Mg-III	370.7796	561,798.7000	588,768.9000	K-I	770.1084	0.0000	12,985.1857
Al-III	371.4179	143,713.5000	170,637.3500	O-I	777.4083	73,768.2000	86,631.4540
C-I	373.6840	60,352.6584	87,113.2390	Mg-II	789.8539	80,650.0200	93,310.5900
Ca-II	373.7964	25,414.4000	52,166.9300	Ca-III	790.0592	327,922.8700	340,580.1500
Al-II	373.9074	105,470.9300	132,215.5170	O-I	794.9354	101,147.5260	113,727.1650
S-II	373.9261	133,360.8600	160,104.1100	O-I	794.9734	101,135.4070	113,714.4440
Fe-I	375.0551	7376.7640	34,039.5160	Na-I	818.5505	16,956.1703	29,172.8870
Fe-I	376.1118	19,390.1680	45,978.0080	Ca-III	819.7588	347,344.3700	359,543.0800
Si-III	379.7202	175,263.1000	201,598.2800	O-I	822.4084	101,135.4070	113,294.8160
Si-III	380.7606	175,336.2600	201,599.4800	K-I	825.2432	21,534.6800	33,652.3200
Fe-I	380.8618	17,927.3820	44,183.6280	K-I	825.4004	21,536.9880	33,652.3200
Mg-I	383.3391	21,870.4640	47,957.0270	O-I	844.8568	76,794.9780	88,631.3030
Mg-I	383.9381	21,911.1780	47,957.0450	O-I	844.8680	76,794.9780	88,631.1460
Si-II	385.7111	55,325.1800	81,251.3200	Ca-II	850.0358	13,650.1900	25,414.4000
Si-II	386.3691	55,309.3500	81,191.3400				

References

1. Clegg, S.M.; Wiens, R.; Misra, A.K.; Sharma, S.K.; Lambert, J.; Bender, S.; Newell, R.; Nowak-Lovato, K.; Smrekar, S.; Dyar, M.D.; et al. Planetary Geochemical Investigations Using Raman and Laser-Induced Breakdown Spectroscopy. *Appl. Spectrosc.* **2014**, *68*, 9. [CrossRef] [PubMed]
2. Taylor, E.J.; Jackson, G.S. Perseverance Rover Lands on Mars. *Electrochem. Soc. Interface* **2021**, *30*, 2. [CrossRef]
3. Wan, X.; Li, C.H.; Wang, H.P.; Xu, W.M.; Jia, J.J.; Xin, Y.J.; Ma, H.Z.; Fang, P.P.; Ling, Z.C. Design, Function, and Implementation of China's First LIBS Instrument (MarSCoDe) on the Zhurong Mars Rover. *At. Spectrosc.* **2021**, *42*, 6. [CrossRef]
4. He, W.X. The study of Laser-Induced Breakdown Spectroscopy. Ph.D. Thesis, Xi'an Institute of Optics and Precision Mechanics of Chinese Academy of Sciences, Xi'an, China, 2011.
5. Aragón, C.; Aguilera, J.A. Characterization of laser induced plasmas by optical emission spectroscopy: A review of experiments and methods. *Spectrochim. Acta Part B At. Spectrosc.* **2008**, *63*, 9. [CrossRef]
6. Bengoechea, J.; Aragón, C.; Aguilera, J.A. Asymmetric Stark broadening of the Fe I 538.34 nm emission line in a laser induced plasma. *Spectrochim. Acta Part B At. Spectrosc.* **2005**, *60*, 7. [CrossRef]
7. Harris, R.D.; Cremers, D.A.; Khoo, C.; Benelli, K.M. LIBS-based detection of geological samples at low pressures (<0.0001 Torr) for Moon and asteroid exploration. In Proceedings of the 36th Annual Lunar and Planetary Science Conference, League City, TX, USA, 1 January 2005.
8. Cousin, A.; Forni, O.; Maurice, S.; Gasnault, O.; Fabre, C.; Sautter, V.; Wiens, R.C.; Mazoyer, J. Laser induced breakdown spectroscopy library for the Martian environment. *Spectrochim. Acta Part B At. Spectrosc.* **2011**, *66*, 805–814. [CrossRef]
9. Zhang, S. Research on Laser Induced Breakdown Spectroscopy in Low Pressure and Calibration-Free Quantitative Method. Master's thesis, Tsinghua University, Beijing, China, 2017.
10. Luo, H.Y.; Shi, H.L.; Li, Z.W.; Li, S.; Xiong, W.; Hong, J. Effect of temperature on performance of space-borne heterodyne interferometer. *Spectrosc. Spectr. Anal.* **2014**, *34*, 2578–2581.
11. Wiens, R.C.; Maurice, S.; Lasue, J.; Forni, O.; Anderson, R.B.; Clegg, S.; Bender, S.; Blaney, D.; Barraclough, B.L.; Cousin, A.; et al. Pre-flight calibration and initial data processing for the ChemCam laser-induced breakdown spectroscopy instrument on the Mars Science Laboratory rover. *Spectrochim. Acta Part B At. Spectrosc.* **2013**, *82*, 1–27. [CrossRef]
12. Maurice, S.; Wiens, R.C.; Saccoccio, M.; Barraclough, B.; Gasnault, O.; Forni, O.; Mangold, N.; Baratoux, D.; Bender, S.; Berger, G.; et al. The ChemCam Instrument Suite on the Mars Science Laboratory (MSL) Rover: Science Objectives and Mast Unit Description. *Space Sci. Rev.* **2012**, *170*, 95–166. [CrossRef]
13. Maurice, S.; Wiens, R.C.; Bernardi, P.; Caïs, P.; Robinson, S.; Nelson, T.; Gasnault, O.; Reess, J.M.; Deleuze, M.; Rull, F.; et al. The SuperCam Instrument Suite on the Mars 2020 Rover: Science Objectives and Mast-Unit Description. *Space Sci. Rev.* **2021**, *217*, 3. [CrossRef]
14. Carter, D.A.; Thompson, W.R.; Taylor, C.E.; Pemberton, J.E. Frequency/Wavelength Calibration of Multipurpose Multichannel Raman Spectrometers. Part II: Calibration Fit Considerations and Calibration Standards. *Appl. Spectrosc.* **1995**, *49*, 11. [CrossRef]
15. Holy, J.A. Determination of spectrometer-detector parameters from calibration spectra and the use of the parameters in spectrometer calibrations. *Appl. Spectrosc.* **2004**, *58*, 10. [CrossRef] [PubMed]
16. Asimellis, G.; Giannoudakos, A.; Kompitsas, M. Accurate wavelength calibration in the near-infrared for multielement analysis without the need for reference spectra. *Appl. Opt.* **2006**, *45*, 35. [CrossRef] [PubMed]
17. Song, Q.; Zhang, T.; Wang, Z.H.; Zhang, S.H.; Yang, L. Intelligent and automatic wavelength calibration method. *Appl. Opt.* **2018**, *57*, 24. [CrossRef] [PubMed]
18. Anderson, R.B.; Forni, O.; Cousin, A.; Wiens, R.C.; Clegg, S.M.; Frydenvang, J.; Gabriel, T.S.J.; Ollila, A.; Schröder, S.; Beyssac, O.; et al. Post-landing major element quantification using SuperCam laser induced breakdown spectroscopy. *Spectrochim. Acta Part B At. Spectrosc.* **2021**, *188*, 106347. [CrossRef]
19. Xu, W.M.; Liu, X.F.; Yan, Z.X.; Li, L.N.; Zhang, Z.Q.; Kuang, Y.W.; Jiang, H.; Yu, H.X.; Yang, F.; Liu, C.F.; et al. The MarSCoDe Instrument Suite on the Mars Rover of China's Tianwen-1 Mission. *Space Sci. Rev.* **2021**, *217*, 58. [CrossRef]
20. Wan, X.; Yuan, R.; Wang, H.P.; Cheng, Y.L.; Jia, J.J.; Shu, R.; Xu, W.M.; Li, C.H.; Xin, Y.J.; Ma, H.Z.; et al. Elastic Particle Swarm Optimization for MarSCoDe Spectral Calibration on Tianwen-1 Mars Rover. *Anal. Chem.* **2021**, *93*, 22. [CrossRef]
21. NIST LIBS Database. Available online: http://physics.nist.gov/PhysRefData/ASD/LIBS/libs-form.html (accessed on 28 September 2022).
22. Stetzler, J.; Tang, S.; Chinni, R.C. Plasma Temperature and Electron Density Determination Using Laser-Induced Breakdown Spectroscopy (LIBS) in Earth's and Mars's Atmospheres. *Atoms* **2020**, *8*, 50. [CrossRef]
23. Nier, A.O.; McElroy, M.B. Structure of the Neutral Upper Atmosphere of Mars: Results from Viking 1 and Viking 2. *Science* **1976**, *194*, 4271. [CrossRef] [PubMed]
24. Kennedy, J.; Eberhart, R.C. Particle Swarm Optimization. In Proceedings of the ICNN'95—International Conference on Neural Networks, Perth, Australia, 27 November–1 December 1995.
25. Li, L.N.; Liu, X.F.; Xu, W.M.; Wang, J.Y.; Shu, R. A laser-induced breakdown spectroscopy multi-component quantitative analytical method based on a deep convolutional neural network. *Spectrochim. Acta Part B Atomic Spectrosc.* **2020**, *169*, 105850. [CrossRef]
26. Yang, F.; Xu, W.M.; Cui, Z.C.; Liu, X.F.; Xu, X.S.; Jia, L.C.; Chen, Y.W.; Shu, R.; Li, L.N. Convolutional Neural Network Chemometrics for Rock Identification Based on Laser-Induced Breakdown Spectroscopy Data in Tianwen-1 Pre-Flight Experiments. *Remote Sens.* **2022**, *14*, 5343. [CrossRef]